Technical Paper

ISSN 1997-1400 Int. J. Pavement Res. Technol. 4(3):185-194

Understanding Vibratory Asphalt Compaction by Numerical Simulation

Kaiming Xia[1+] and Tongyan Pan[2]

Abstract: Asphalt compaction involves a reduction in the volume of hot mixture asphalt layer, which has been considered as one of the most important factors affecting the future mechanical performance of flexible pavement system. It should be the essential part of the intelligent asphalt compaction. So far, little research work has been reported on modeling vibratory asphalt compaction. In this paper, the underpinning principles of finite element for asphalt compaction simulation are briefly introduced. A three dimensional finite element model for vibratory asphalt compaction is presented. In order to predict spatial density, geometric nonlinearity capturing the configuration change is employed to simulate the compaction process. The low compressible hot mixture asphalt is modeled as rate dependent crushable foam model with volumetric hardening. Numerous simulations of vibratory asphalt compaction considering different compactor operations are conducted to understand their impacts on the compacted density.

***Key words**: Compacted density; Finite element; Operation parameters; Vibratory asphalt compaction.*

Introduction

Compaction is the mechanical process of densifying and reducing the volume of material [1]. It has been understood that achieving appropriate compaction at the time of construction is very critical to the future performance of an asphalt pavement [2]. During the construction of an asphalt pavement, subgrade soil, aggregate bases, and hot mixture asphalt are all needed to be compacted. Improper compaction during construction is a leading cause of asphalt pavement degradation. For asphalt mixture, compaction locks the asphalt-coated aggregate particles together and provides resistance to deformation (or rutting) while simultaneously reducing permeability and improving durability. A fully compacted subgrade soil and asphalt layer will also reduce the chance to develop consolidation rutting after putting into service. Mechanical compaction is considered as an important approach to removing air voids. Adequate compaction of asphalt mixture is essential: (1) to prevent further significant densification under traffic, (2) to provide adequate shear strength, (3) to ensure that asphalt mixture is nearly waterfproof, (4) to prevent excessive oxidation of the asphalt binder resulting in subsequent cracking.

During the asphalt compaction process, energy is transferred to hot mixed asphalt (HMA) layers through the rolling drum, which causes the geomaterial particles to stack closer together. The void between the particles is reduced under the external loads. For pavement material, the critical engineering properties of asphalt are resilient modulus, compressibility, and permeability, which are closely related to asphalt compaction. Compaction of the asphalt mixture generally increases its resilient modulus, and decreases compressibility and permeability. In pavement engineering, hot mixed asphalt layer can be efficiently compacted using all kinds of compaction equipment [1, 3]. The compaction equipment includes pneumatic or rubber tired compactor, tipped compactor, and vibratory compactor. Vibratory compactors have been considered as a robust tool for compacting sand geomaterial while static compactor is generally used for compacting clay. Smooth drums installed with vibratory system have been widely used to compact hot mixture asphalt. Vibratory compactor generally uses rotating eccentric masses within the drum, which can transfer additional energy to the ground to increase compaction effort. The roller generally overlaps each pass a little bit to ensure that the target density is achieved completely throughout the HMA layer. After compaction pass, the compaction density can be tested through nuclear density gauge at the construction sites.

During the past few decades, both soil and asphalt compactions have received some attention in the field of pavement engineering. The research efforts were generally focused on experimental device developments and field testing [1, 3]. Some analytical and empirical approaches on asphalt compaction were also investigated [3-6]. These developments have facilitated the development of asphalt compaction technology and qualitative understanding asphalt compaction, which are beneficial to pavement construction. However, these analytical models oversimplify the dynamic roller interaction and fail to describe the dynamic compaction processes. It is evident to pavement researchers that more efforts need to be devoted to developing robust computer models so that dynamic asphalt compaction can be simulated easily. Intelligent asphalt compaction procedures can be determined based on numerical simulations. Based on the available literature on soil/asphalt compaction, it seems to be true that very little work has been done to understanding soil/asphalt compactions in pavement engineering [7]. As a robust numerical method, finite element has been widely used to study pavement structure. Given the theoretical framework of large deformation, finite element method can be effectively applied to predict soil/asphalt compaction in terms of spatial density change. On the numerical modeling of soil/asphalt compaction, the author did some initial research work on this topic [1, 8] as well as other researchers [9, 10, 11]. To better model HMA, a thermomechanical constitutive model is presented in literature [7] and numerical simulation of gyratory compaction experiments in

[1] Division of Engineering, Colorado School of Mines, Golden CO 80401, USA.
[2] Department of Civil Engineering, The Catholic University of America, Washington, DC 20064, USA.
[+]Corresponding Author: E-mail kaiming.xia@gmail.com
Note: Submitted May 5, 2010; Revised August 25, 2010; Accepted August 31, 2010.

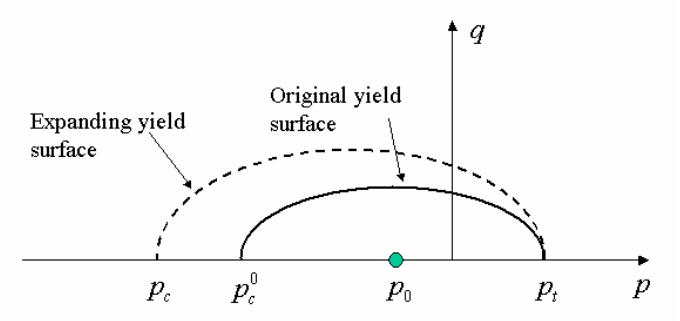

Fig. 1. Crushable Foam Type Material Model.

terms of displacement is provided. Other numerical approach with discrete element was explored in [12]. The literature survey shows very few papers focused on modeling asphalt compaction have been published in the past. The main purpose of this paper is to present an advanced finite element model for asphalt compaction. Different machine operation factors involving vibratory asphalt compaction are investigated, which demonstrate the finite element model can be efficiently used to predict the most concerned issue of asphalt compaction in terms of density change. This was rarely reported in the past. The author believes this topic should be the major issue of intelligent compaction.

Prediction of Compacted Density and Material Model

In order to predict the density change, it is necessary to recognize that the deformation of the geomaterial medium could be relatively large during a loading-unloading cycle. This necessitates the clear distinguishing between the undeformed configuration and deformed configuration after geomaterial compaction. For a typical time step, the updated configuration of the body at step $t_n + \Delta t$ may be written as a function of the configuration at step t_n and the incremental displacement Δu during the time-step Δt. The current configuration can be given as

$$X_{n+1} = X + u = X_n + \Delta u \tag{1}$$

where **u** is the total displacement vector with respect to the original configuration. The deformation gradient is defined as follows:

$$\mathbf{F} = \frac{\partial \varphi}{\partial \mathbf{X}} = \mathbf{1} + \frac{\partial \mathbf{u}}{\partial \mathbf{X}} \tag{2}$$

where **1** is the identity unit tensor. Ω_t denotes the current configurations for updated Lagrangian formulation and their relationship with the reference configuration Ω_0. Based on the mass conservation, the volume relationship between reference and current configurations can be established as

$$d\Omega_{n+1} = \det \mathbf{F}_{n+1} d\Omega_0 = J_{n+1} d\Omega_0 \tag{3}$$

Therefore, with the large deformation updated Lagrangian formulation, one can predict the density change or compaction. In updated Largrangian formulation, an incremental displacement is defined with respect to the configuration at time t_n, which is considered as the reference configuration for the current load step. The updated Lagrangian formulation can therefore be visualized as a series of intermediate total Lagrangian formulation. The relative compaction density can be updated at time t_{n+1} by

$$\rho_{n+1} = \frac{\rho_0}{\mathrm{Det}F_{n+1}} \quad \text{or} \quad \rho_{n+1} = \frac{\rho_n}{\mathrm{Det}f_{n+1}} \tag{4}$$

Here ρ_0 is the initial density and ρ_{n+1} is the relative density at time step t_{n+1}. Therefore, large deformation analysis has many advantages in predicting geomaterial compaction in civil engineering.

For modeling compaction, the material model should contain volumetric hardening capability. A volume-preserving plastic model cannot be used to simulate compaction, such as Von Mises model. Since asphalt can exhibit relatively small tensile strength during compaction, a rate dependent yield crushable foam model integrated in commercial finite element software ABAQUS is selected for asphalt compaction simulations [13]. The model allows a different response in compression and tension. The foam model contains volumetric hardening, which can be easily calibrated for modeling the compaction process of HMA. The foam model with volumetric hardening is shown in Fig. 1.

The yield surface and plastic flow potential for the foam models are defined as follows:

$$f = \sqrt{q^2 + \alpha^2 (p - p_0)^2} + B = 0 \tag{5}$$

$$g = \sqrt{q^2 + \beta^2 p^2} \tag{6}$$

The parameter α is a function of yield stress ratios for compression loading and hydrostatic loading and given by

$$\alpha = \frac{3k}{\sqrt{(3k_t + k)(3 - k)}}, \qquad k = \frac{\sigma_c^0}{p_c^0}, \qquad k_t = \frac{p_t}{p_c^0} \tag{7}$$

p is defined as the pressure stress

$$p = \frac{1}{3}\mathrm{tr}\boldsymbol{\sigma} = K\mathrm{tr}\boldsymbol{\varepsilon} \tag{8}$$

tr denotes trace operator. And, q is the Mises stress defined as follows:

$$q = \sqrt{\frac{3}{2}\mathbf{s} : \mathbf{s}} = \sqrt{\frac{3}{2}}\|\mathbf{s}\| = \sqrt{3J_2(\mathbf{s})} \tag{9}$$

Both yield function and flow potential represent as an ellipse in the $I_1 - \|\eta\|$ stress plane with α and β representing the shape of the yield ellipse and the flow potential, respectively; the shape factor, α, remains as a constant during plastic deformation process; p_0 is the center of the yield surface and defined as $p_0 = (p_c + p_t) / 2$, and B is the length of the vertical q-axis of the yield ellipse and calculated by $B = \alpha(p_c - p_t) / 2$. For the volumetric hardening model, the evolution of the yield surface of ellipse is governed by the volumetric compaction plastic strain, ε_{vol}^p. Also the volumetric hardening model assumes that the hydrostatic tension strength, p_t is

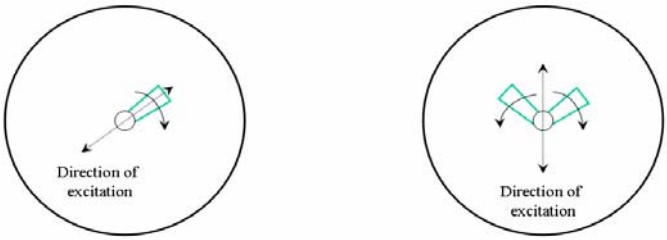

Fig. 2. Vibratory Drum with Different Setting of Direction of Excitation.

constant throughout the plastic deformation process. The yield surface expands by increasing $p_c\left(\varepsilon_{vol}^{p}\right)$ as a result of compaction when the material's density is increased or shrunk once the material's density is reduced. This constitutive model is used to define the HMA material behavior during compaction.

Vibratory Asphalt Compaction

There are four types of rollers used for compacting asphalt mixtures: static, vibratory, pneumatic, and combination. A static roller uses the machine's weight to compact geomaterials. A vibratory roller uses a combination of static and vibratory force. The compaction effort caused by static roller comes from the weight of the roller frame and drums. The compaction effort caused by vibratory forces is improved by a rotating eccentric mass inside each drum. As the eccentric mass rotates around an axle located inside the drum (the axle is independent of the wheel axle), a centrifugal force is produced (see Fig. 2). The vibratory force is calculated by

$$F(t) = M_0 e_0 \omega^2 \tag{10}$$

where M_0 is the eccentric mass, e_0 is the distance between the center of eccentric mass and its axle, and ω is the angular velocity. The frequency and the amplitude of vibration produced by the vibratory roller are the two components of the vibratory force, which can be adjusted for intelligent compactor. The vibratory force $F(t)$ can be decomposed into two components $F_x(t)$ and $F_y(t)$.

The frequency of vibrations can be controlled by operator, and different compactors in the market have different settings. For asphalt compaction, the vibratory roller should be operated at a relatively higher frequency of 40Hz. Certainly the frequency cannot be too high that can cause drum to loose contact with ground and lead to non uniform compaction. Also it can make the operator feel uncomfortable. As the frequency decreases and the roller's speed increases, the number of impacts per meter will decrease and relatively less energy is transferred to ground. If the vibratory roller is operating at the highest possible frequency, the roller's speed will be the determining factor to control the number of impacts per meter. For asphalt compaction, the greater the number of impacts per meter, the greater the compaction effort can be achieved by the vibratory roller. Impacts per meter N are determined by dividing the frequency of vibration force f_V by the roller's speed V_x,

$$N = \frac{f_V}{V_x} \tag{11}$$

The vibratory compaction has been used many years in pavement construction for either subgrade soil or asphalt layer. Qualitatively understanding vibratory asphalt compaction might have been achieved in pavement engineering. However, accurately predicting different machine operations on asphalt compaction in terms of density change has rarely been investigated.

Finite Element Model for Asphalt Compaction

The author wants to emphasize the finite element model for vibratory asphalt compaction presented in this paper is created for purely research purpose, which does not represent any real asphalt compactors currently used in pavement engineering. For comparison, two types of rollers are modeled for compacting HMA: non-vibratory (static compaction) and vibratory compactions. For vibratory compaction, the vibratory force is generated using the first option in Fig. 2. In this example, the author assumes the asphalt compactor has two drums. The two drums are connected by constant distance. The machine frame is modeled as a rigid body and a point mass element is defined at the centroid's position and a gravity force is applied at the centroid. Fig. 3 is the finite element model for non-vibratory and vibratory asphalt compactions. Rolling compaction is simulated to demonstrate the advantage of the developed FEA compaction model. In order to reduce the number of elements, a symmetric FEA model is used. Fine mesh is used for the compaction area and relatively coarse mesh is defined outside the contact domain. The analyzed domain for the compaction model is 10.0 m in the rolling direction, the width is 3.0 m, and the depth is 2.0 m for subgrade soil, 0.3 m for base, and 0.125 m for HMA layer. The boundary conditions are fully fixed at the bottom of subgrade soil and only fixed in the normal direction with other surfaces as shown in Fig. 3. For the geometry of the roller, the diameter is 1.3m and 1.72m in width. The wheel base is 3.44 m. The dead load acting on the rear axle is 48432 N and the front axle load is 49647 N, which are simulated by applying vertically at the wheel center. The angular velocity is applied at the axles to drive the compactor rolling forward and backward.

The initial density for the HMA layer is assumed to be 2.2 ton/m^3. The Young's modulus E and the Poisson's ratio v are 30.0 MPa and 0.3, respectively. For modeling compaction, the foam model with volumetric hardening is used to model asphalt compaction (see Fig. 4). The compression yield stress ratio is 2.0 and the hydrostatic yield stress ratio is 0.4. The damping properties for HMA are the Rayleigh mass proportional damping coefficient α = 100 s^{-1} and the Rayleigh stiffness proportional damping, β = 0.0002 s. For the base layer, the density is 2.4 ton/m^3 and assumed to deform elastically. The Young's modulus E and the Poisson's ratio v are 150MPa and 0.3, respectively. The Rayleigh damping properties are the mass proportional damping coefficient α = 10 s^{-1} and the stiffness proportional damping, β = 0.0005 s. The subgrade soil is assumed to deform elastically. In this example study, the eccentric mass moment is assumed to be m_0e_0 = 1.585 kg·m. The vibratory force frequency is 40Hz. The rotation of eccentric mass will generate both horizontal and vertical excitation force components, which is dependent on the eccentric mass moment and angular velocity. For non-vibratory compaction, only the machine weight is considered.

The goal in compacting HMA is to produce a smooth, stable and

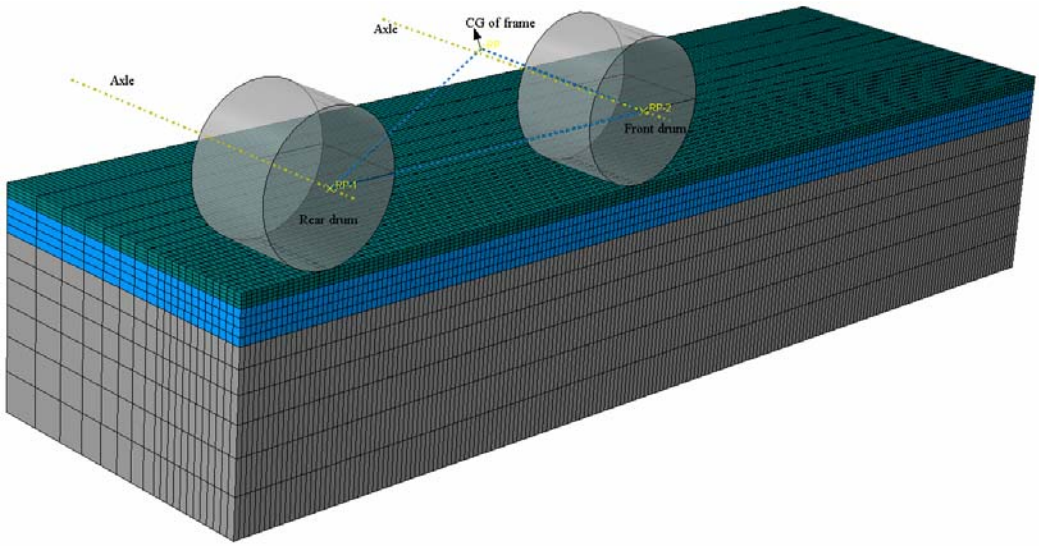

Fig. 3. Finite Element Model for Vibratory Asphalt Compaction.

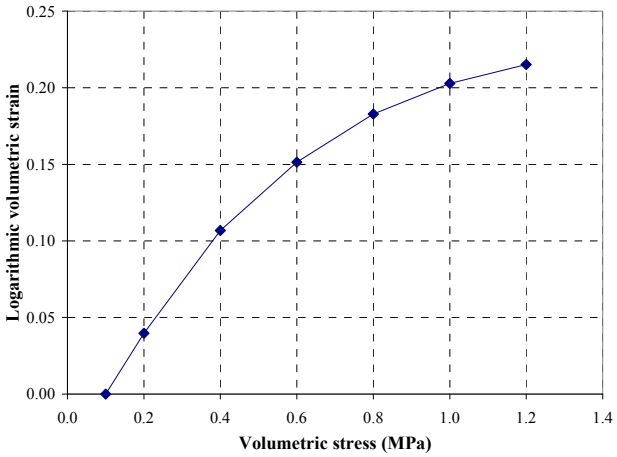

Fig. 4. Volumetric Hardening Curve for Asphalt Mixture.

durable asphalt pavement. Understanding the factors affecting asphalt compaction represents an important step to achieve this goal. There are many factors that affect the final asphalt compaction. Among those possible factors are the properties of the asphalt mixture, asphalt type and density of the underlying base course material, the thickness of asphalt layers, and the environmental conditions at the time of placement. If any of these factors change, the compaction requires the operator to adjust the compaction procedures and eventually the final modulus, stiffness or strength of the mix be affected. In this paper, the numerical study is focused on investigating different machine operations on asphalt compaction.

Non-vibratory and Vibratory Asphalt Compaction

For vibratory compaction, both horizontal and vertical vibratory forces are applied at the wheel centers. A 5-pass compaction is simulated for both non-vibratory and vibratory compaction. Fig. 5 is the vertical stress projected onto the deformed configuration at the very beginning, in which a stress bulb is exhibited and induced by the total dead load. Figs. 6-8 show the vertical stress contours projected onto the deformed configuration during compaction process. Stress bulbs can be easily seen throughout the compaction, but vary a lot due to the cyclic vibratory excitation at different instants. As mentioned earlier, finite element can be used to calculate the spatial density using large deformation formulation. Fig. 9 and Fig. 10 show the spatial density contours projected onto the current configuration for both non-vibratory and vibratory compactions. Based on Fig. 9 and Fig. 10, one can see that spatial density contours projected onto the current configurations for non-vibratory is relatively smaller than that of vibratory compaction. Also for vibratory compaction, the density induced by three compaction passes is larger than that after two compaction passes (see Fig. 10 and Fig. 11). For the numerical example, the initial density of HMA layer is 2.2 ton/m^3. After first compaction pass, the maximum density changes from 2.2 ton/m^3 to 2.679 ton/m^3 for non-vibratory compaction and to 2.690 ton/m^3 for vibratory compaction. Fig. 12 shows the comparative study of the vertical displacement of the wheel center for both non-vibratory and vibratory compactions. Also the frequency of the vertical displacement is exactly same as that of vibratory force. Due to the additional vibratory force, the vertical displacement induced by vibratory compaction is larger than that of non-vibratory compaction, which is also be reflected in the density change. One also should understand that large settlement has no direct relationship with asphalt compacted density. The density change should be strictly dependent on the volumetric change.

Permanent compaction is generated under two conditions: HMA exhibits plastic deformation and the volume of HMA is reduced too. During the asphalt compaction process, plastic dissipation, to some extent, can be used to estimate how much energy is transferred to HMA layer to generate compaction. Higher plastic dissipation indicates more energy is transferred to HMA to generate permanent deformation. Fig. 13 shows the plastic dissipation of HMA layer versus the number of compaction passes. It also shows that, with additional vibratory force, vibratory compaction transfers a relatively more energy to HMA layer than that of a non-vibratory compaction. This is consistent with the result on compacted density (see Fig. 14). Based on all these results, it can be easily seen that vibratory compaction generates a higher compacted density on

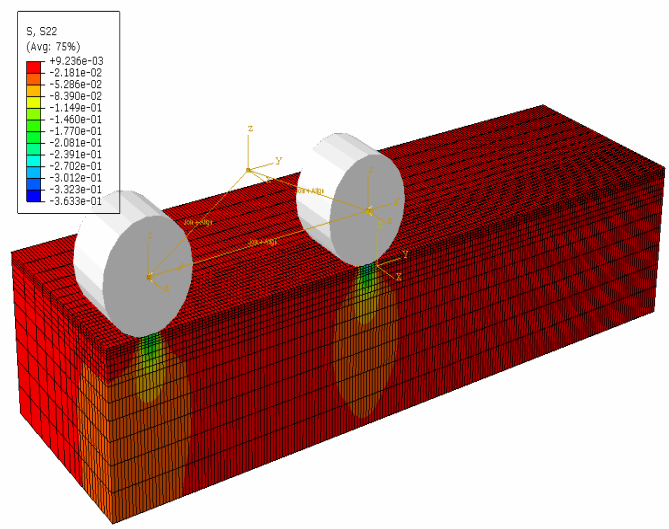

Fig. 5. Vertical Stress Contour Projected onto the Deformed Configuration before Rolling Compaction.

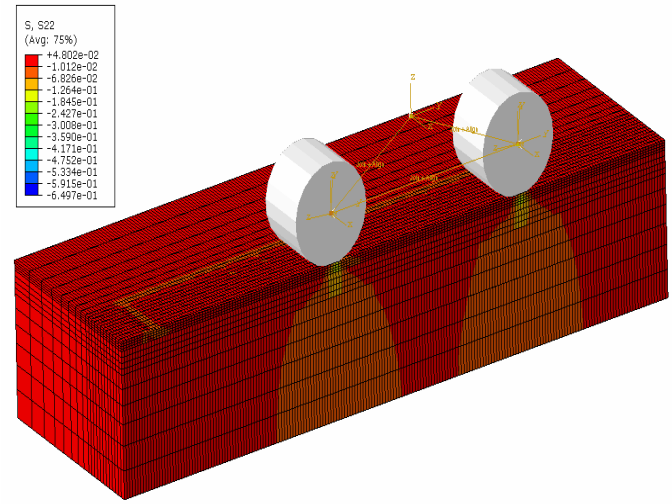

Fig. 6. Vertical Stress Contour Projected onto the Deformed Configuration for Vibratory Compaction.

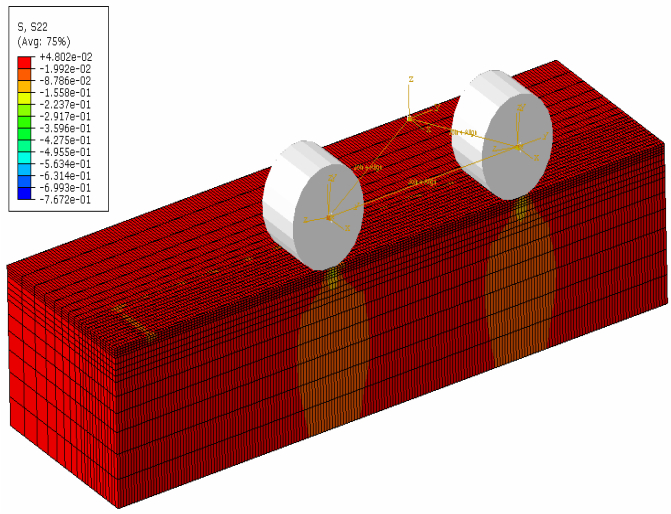

Fig. 7. Vertical Stress Contour Projected onto the Deformed Configuration for Vibratory Compaction.

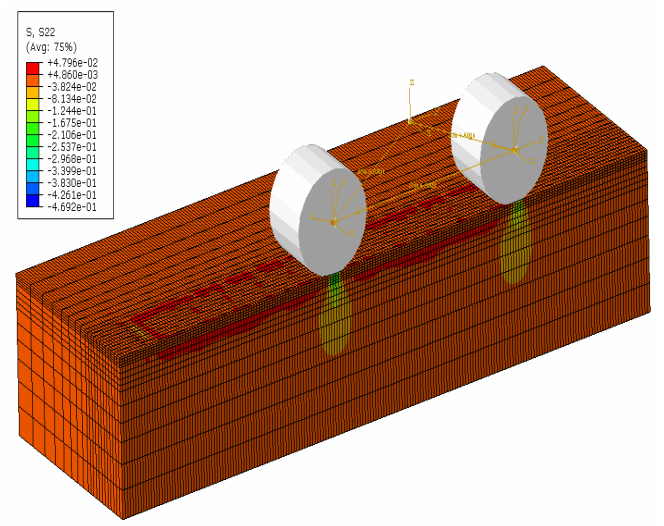

Fig. 8. Vertical Stress Contour Projected onto the Deformed Configuration for Vibratory Compaction.

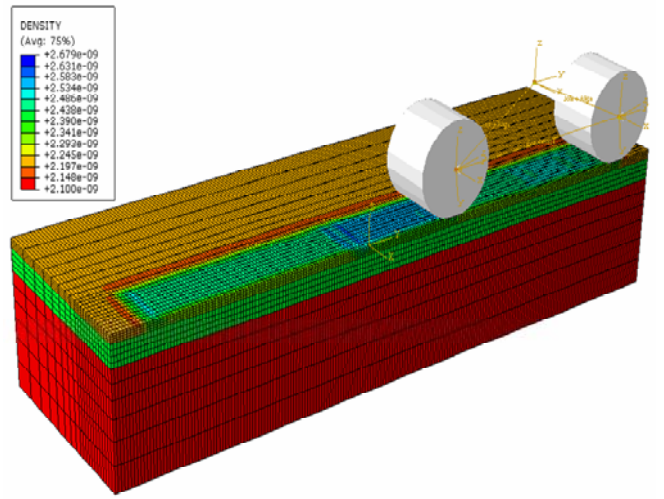

Fig. 9. Spatial Density Contour Projected onto the Deformed Configuration for Non-vibratory Compaction (First Pass).

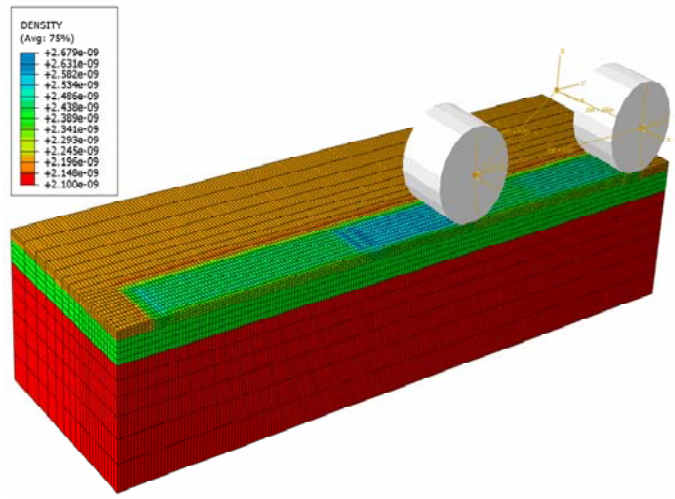

Fig. 10. Spatial Density Contour Projected onto the Deformed Configuration for Vibratory Compaction (the Horizontal Force is Zero, after 1 Compaction Pass).

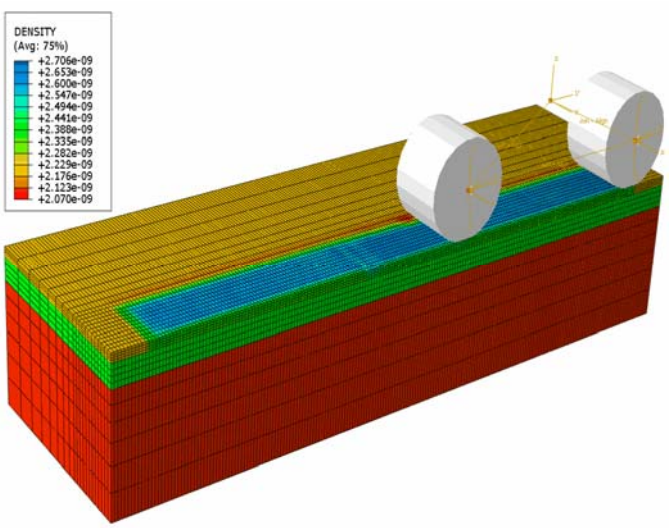

Fig. 11. Spatial Density Contour Projected onto the Deformed Configuration for Vibratory Compaction (the Horizontal Force is Zero, after Three Compaction Passes).

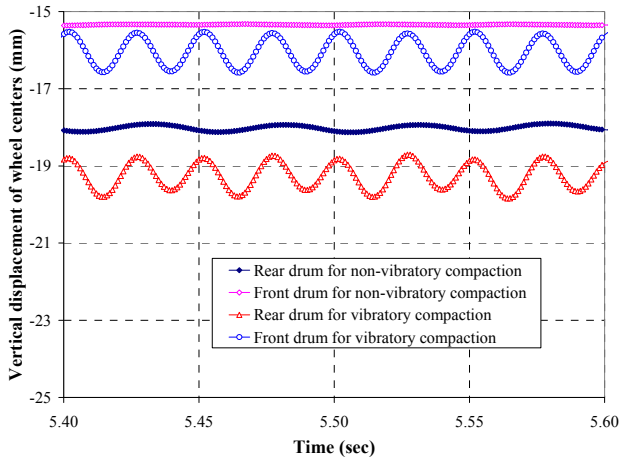

Fig. 12. The Vertical Displacement of Two Wheel Centers for Case A and Case B (Forward Compaction of Pass 1).

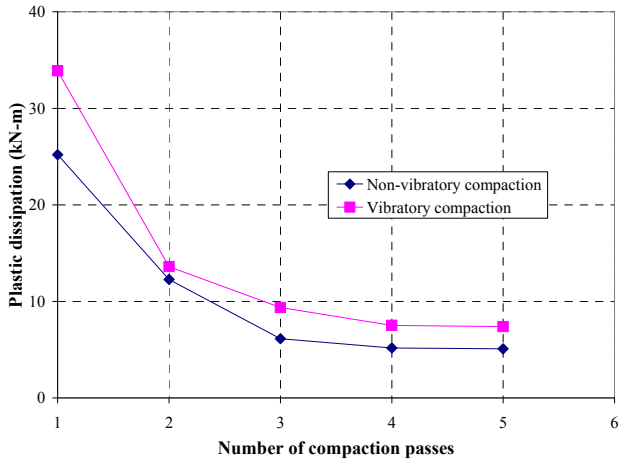

Fig. 13. Plastic Dissipation for Non-vibratory and Vibratory Compaction.

HMA layer than that of non-vibratory compaction. Fig. 14 shows the largest amount of compaction taking place during the first

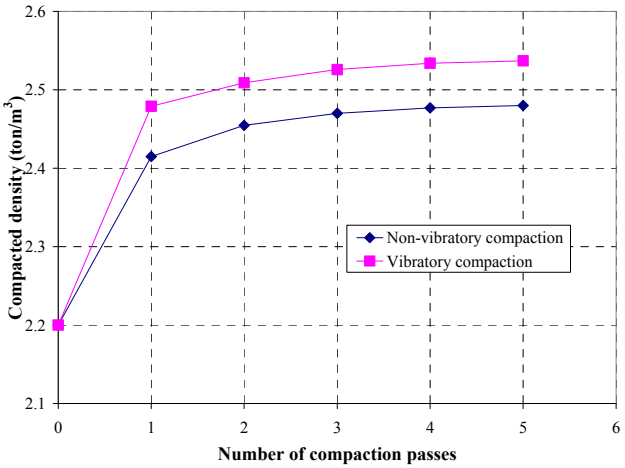

Fig. 14. Compaction Density Versus Number of Compactor Passes.

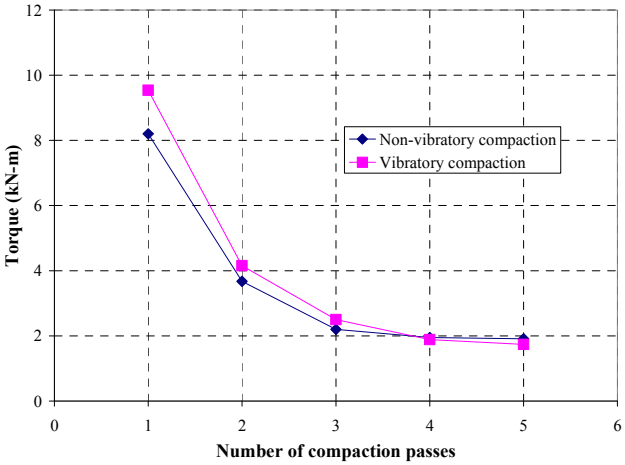

Fig. 15. Axle Torque Versus the Number of Compaction Passes.

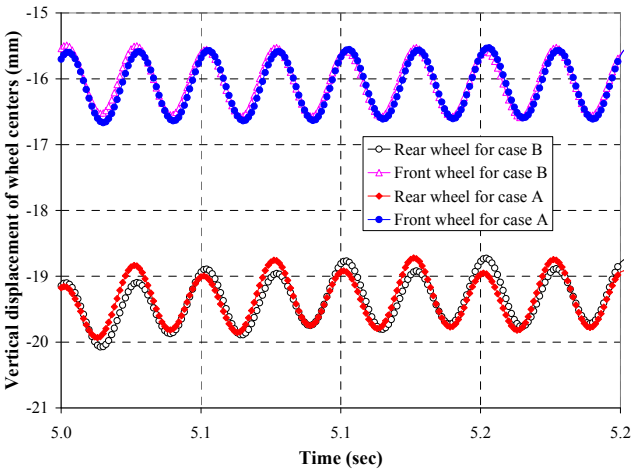

Fig. 16. The Vertical Displacement of Two Wheel Centers for Case A and Case B (Forward Compaction of Pass 1).

compaction pass and further compaction will diminish with subsequent compaction passes. After a certain number of compaction passes, the density will stabilize at an approximately constant level without considering the rate dependent material behavior. The compacted densities from both cases gradually increase and converge to constant values, which indicate compacted

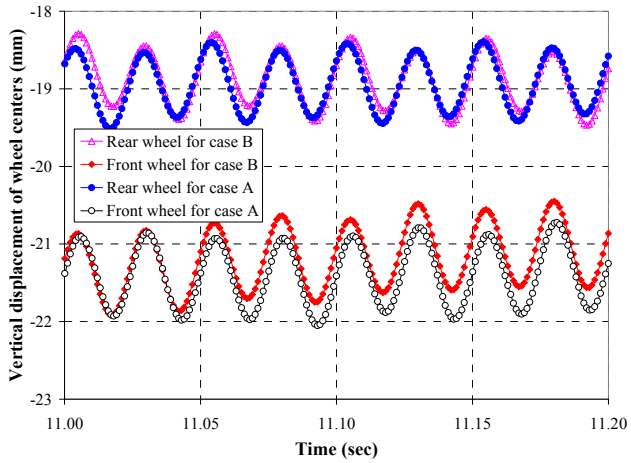

Fig. 17. The vertical displacement of two wheel centers of case A and case B (reverse compaction of pass 2).

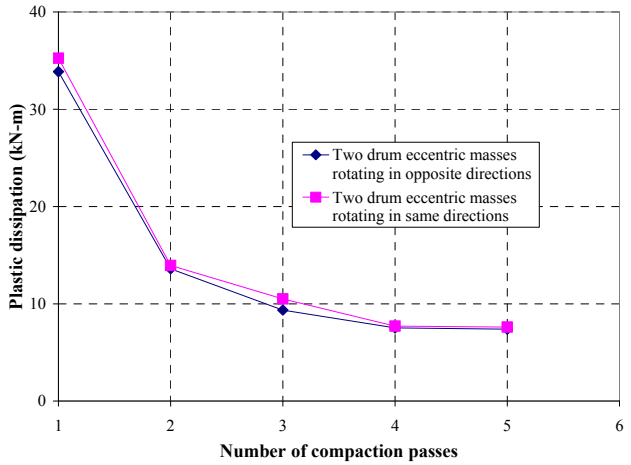

Fig. 18. Plastic Dissipation Versus Number of Compaction Passes.

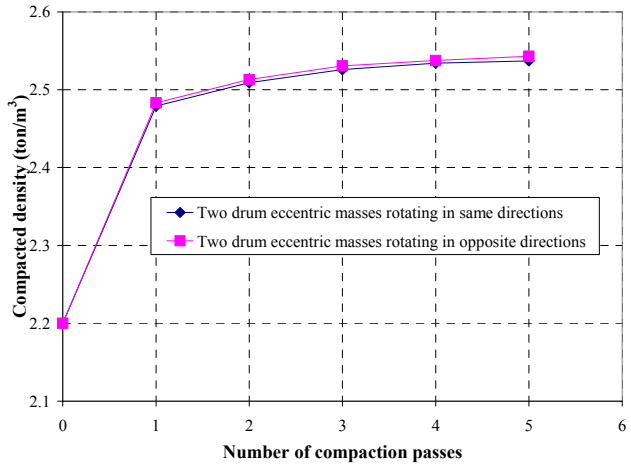

Fig. 19. Comparison of Compacted Density for Different Rotation of Two Drum Eccentric Masses.

density has a clear upper limit for each case. The results show that the maximum achievable densities for non-vibratory compaction and vibratory compaction are not same. The reason can be on two aspects. Theoretically the maximum density of HMA can be obtained when its void ratio reaches zero. During the compaction

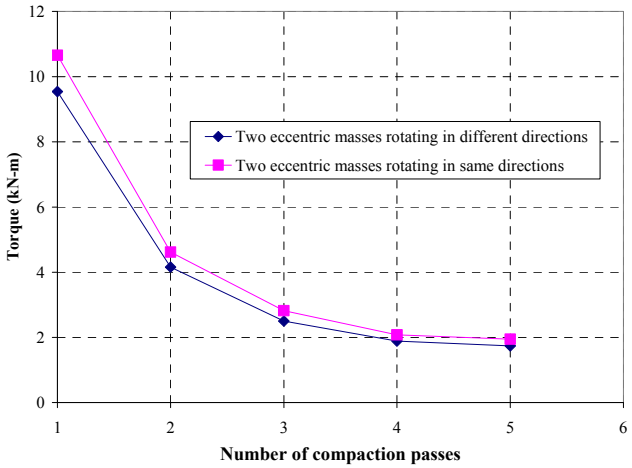

Fig. 20. Comparison of Axle Torque for Different Rotation of Two Drum Eccentric Masses.

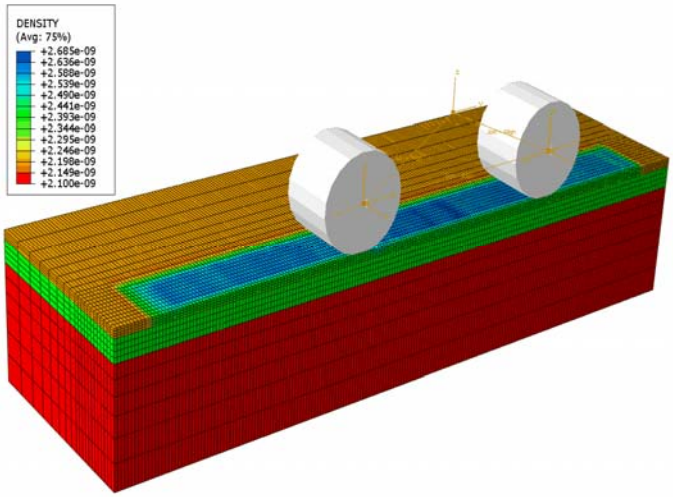

Fig. 21. Spatial Density Contour Projected onto the Deformed Configuration for Vibratory Compaction of Case A (During the Third Pass).

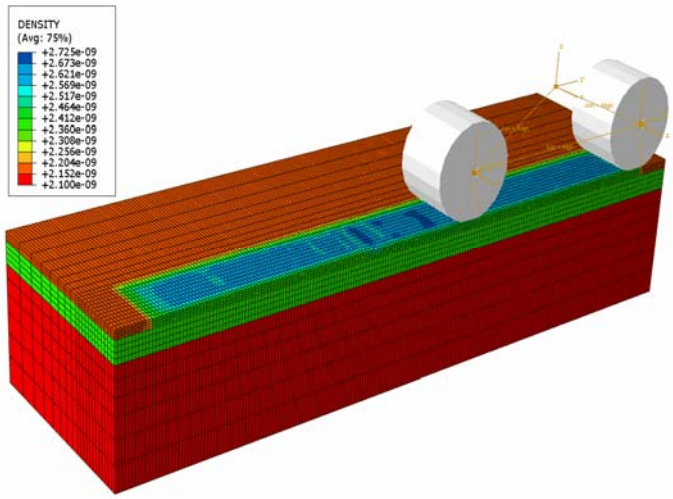

Fig. 22. Spatial Density Contour Projected onto the Deformed Configuration for Vibratory Compaction of Case B (after Third Pass).

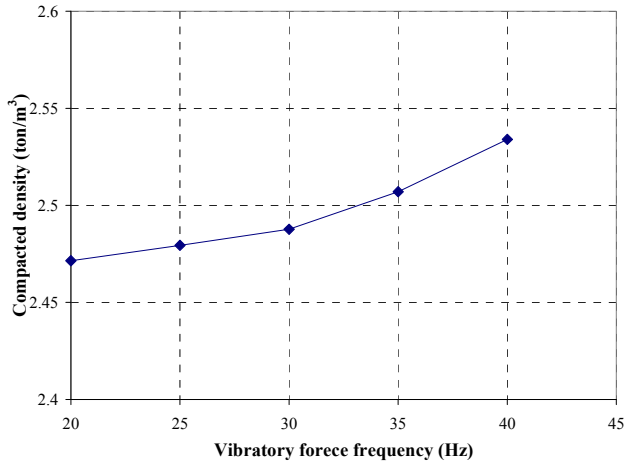

Fig. 23. Compaction Density Versus Vibratory Force Frequency.

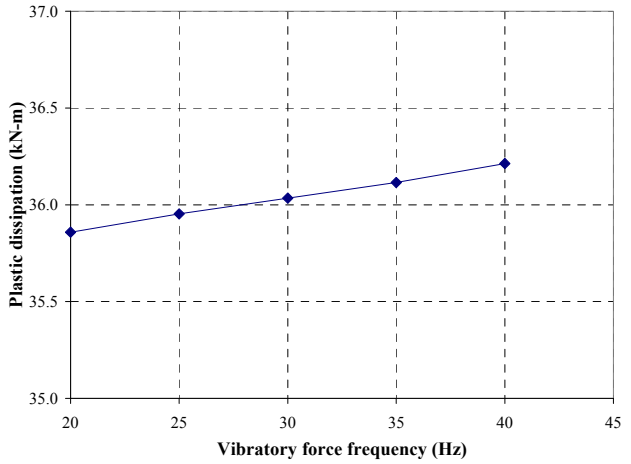

Fig. 24. Plastic Dissipation versus Vibratory Force Frequency.

process, the spatial density gradually increases after each compaction pass. However the maximum density corresponding to zero void ratio cannot be achieved ideally. For a given HMA property, lift thickness and compaction equipment, there exists a maximum density that compactor can achieve after certain number of compaction passes. During the compaction process, the interlock of particles is adjusted. The compacted density is increased by a small amount but a critical amount to improve the future pavement performance. Fig. 15 shows the relationship of compactor axle torque versus the number of compaction passes. It indicates that the axle torque gradually decreases and converges to a constant level after a number of compactor passes. This is due to the fact that HMA material becomes stiffer after it is fully compacted. Also the rolling resistance of the wheels decreases, which is reflected in terms of the decreasing trend of axle torque. Fig. 15 shows the axle torque of vibratory compaction becomes lower than that of non-vibratory compaction after the fourth compaction pass. The reason is vibratory compactor compacting HMA layer faster than non-vibratory compactor, and correspondingly the axle torque reduces relatively faster than non-vibratory compactor. While the trend shown in these figures can be easily predicted, the quantitative prediction of these results has rarely been conducted in the past.

Horizontal Components of Vibratory Forces on Asphalt Compaction

For double-drum vibratory compactor, the setting of eccentric masses might be another important factor on compaction. Besides the vertical force, the resulting horizontal components of the vibratory forces generated simultaneously by the front and rear drums on asphalt compaction should be considered and is investigated here. In this example study, the setting of the rotating mass for the front and rear drums are same. Each drum is equipped with single rotating mass. The resulting horizontal components of the vibratory forces induced by the front drum and the rear drum should be minimum or can be neglected if they are rotated at the same angular velocity in opposite directions. Otherwise the resulting horizontal force will be maximum if they are rotated in same direction. This resulting horizontal force drives the compactor cyclically forward-backward during compaction and helps to compact the asphalt mixture uniformly. In this study, a comparative study of the above two cases is conducted. They are defined as case A, which delivers the maximum horizontal excitation force if the eccentric masses are rotated in same direction at the same angular velocity. Case B provides the minimum horizontal excitation force and the eccentric masses are rotated in opposite direction at the same angular velocity. Fig. 16 and Fig. 17 show the vertical displacements of wheel centers for case A and case B. Fig. 16 shows the vertical displacement of the rear wheel center is larger than that of the front wheel center. Fig. 17 shows the vertical displacement of the front wheel center is larger than that of the rear wheel center for the reverse compaction of pass 2. The difference of the vertical displacements between the front wheel and the rear wheel decreases for both case A and case B when the number of compaction passes is increasing. The reason is that HMA layer becomes stiffer after a number of compaction passes. Fig. 18 shows that plastic dissipation of case A is lower than that of case B. Based on the amount of plastic dissipation, one can predict that case B provides relatively better compaction than that of case A. Fig. 19 shows that compacted density of case A is lower than that of case B. Also, it clearly indicates that cyclic horizontal force component can increase compaction. However the total axle torque of case B is relatively higher than that of case A and indicates a higher energy input from compactor, which can be seen in Fig. 20.

Fig. 21 and Fig. 22 are the spatial density contours projected onto the deformed configurations for case A and case B. Based on the Fig. 21 and Fig. 22, one can easily see that case B of rotating two drum eccentric masses in opposite direction increases the compacted density of HMA layer.

Vibratory Force Frequency on Asphalt Compaction

Vibratory force varies by changing the frequency or the eccentric mass moment. For many designs, it is possible to vary both. When changing frequency, the effect on the centrifugal force varies by the square of frequency. However, changing frequency has a direct influence on the impact spacing. Therefore, reducing frequency tends to reduce compaction. Vibratory compaction is more effective than the non-vibratory compaction because it can transfer more energy to HMA layer. Vibratory compaction also helps to facilitate

an even greater interlocking effect afterwards and can greatly reduce mechanical friction during the compaction process. Fig. 23 shows the relationship between compacted density and vibratory force frequency. It shows compacted density increases with increasing vibratory force frequency and eventually converges to constant level. Fig. 24 shows the plastic dissipation also increases with increasing vibratory force frequency, which indicates more energy is transferred to the asphalt mixture to generate permanent deformation.

Concluding Remarks

The mechanical behavior of HMA layer is greatly influenced by the compaction at the time of construction. Compacted density is an important technical parameter to evaluate the compaction in pavement engineering. Higher compaction density always implies a higher resilient modulus and a better mechanical performance for future flexible pavement system. Among the compaction methods, vibratory asphalt compaction delivers a better compaction solution to HMA layer. But vibratory rollers require more strict operation than non-vibratory compaction. Accurately delivering best compaction to HMA is a challenging task because quantifying the asphalt compaction is so many complexities and variables involved. So far, very little research work has been devoted to estimating vibratory asphalt compaction.

In this paper, the underpinning formulation for predicting asphalt compaction is briefly introduced. A three dimensional large deformation finite element model for vibratory asphalt compaction is developed and applied to understand intelligent asphalt compaction procedures. The developed finite element model is used to predict the spatial density change due to rolling compaction, in which the HMA layer is modeled using foam type model. Similar complex finite element modeling of asphalt compaction has not been reported in open literatures. Numerous factors involved with machine operations on asphalt compaction are investigated. For vibratory asphalt compaction, the vibratory frequency is also an important parameter influencing the final asphalt compaction. While the machine travels at a constant speed, increasing vibratory frequency implies a high number of impacts over HMA layer. Thus more energy is transferred to HMA layer and leads to high compaction. Numerical study confirms that vibratory compaction can deliver a better compaction than non-vibratory compaction. This paper offers an advanced finite element model for predicting asphalt compaction, which is an issue of great significance in geotechnical and pavement engineering. For either asphalt compaction or intelligent compaction, it should be aimed at achieving maximum compaction. Any intelligent system development should be centered on this goal. The advanced model presented in this paper will help researchers innovate the intelligent compaction system development and determine the intelligent compaction procedures.

References

1. Xia, K. and Chi, L. (2008). A viscoplastic foam model for prediction of asphalt pavement compaction, *ASCE Geotechnical Special Publication Series, No. 182*, pp. 136-145.
2. Masad, E., Muhunthan, B., Shashidhar, N., and Harman, T. (1999). Quantifying laboratory compaction effects on the internal structure of asphalt concrete, *Transportation Research Record*, No. 1681, pp. 179–185.
3. Pietzsch, D. and Poppy, W. (1992). Simulation of geomaterial compaction with vibratory roller, *Journal of Terramechanics*, 29(6), pp. 585-597.
4. Carman, K. (2008). Prediction of soil compaction under pneumatic tires a using fuzzy logic approach, *Journal of Terramechanics*, 45(4), pp. 103-108.
5. Canillas, E. and Salokhe, V. (2002). Modeling compaction in agricultural soils, *Journal of Terramechanics*, 39(2), pp. 71-84.
6. Montgomery, D. (1999). *Stabilized Soil Research Progress Report SSRPR06*, School of Engineering, University of Warwick, UK.
7. Koneru, S., Masad, E., and Rajagopal, K.R. (2008). A thermomechanical framework for modeling the compaction of asphalt mixes, *Mechanics of Materials*, 40(10), pp. 846-860.
8. Xia, K. and Masud, A. (2009). A stabilized finite element formulation for finite deformation elastoplasticity in geomechanics, *Computers and Geotechnics*, 36(3), pp. 396-405.
9. Brandl, H., Kopf, F., and Adam, D. (2005). Continuous Compaction Control (CCC) with differently dynamic rollers, *Heft 553*, Wien.
10. Mahutka, K. and Grabe, J. (2005). Numerical investigation of soil compaction and vibration propagations due to strong dynamic excitation, *Proceeding of Joint ASME/ASCE/SES Conference on Mechanics and Materials*, June 1-3, 2005, Baton Rouge, Lousiana, USA.
11. Krishnan, J. M. and Lakshmana, Rao C. (2000). Mechanics of air voids reduction of asphalt concrete using mixture theory, *International Journal of Engineering Science*, 38(12), pp. 1331–1354.
12. Wang, L., Zhang, B., Wang, D., and Yue, Z. (2007). Fundamental mechanics of asphalt compaction through FEM and DEM Modeling, *Analysis of Asphalt Pavement Materials and Systems: Engineering Methods*, No. 176, pp. 45-63.
13. ABAQUS Online Document Version 6.9.